Chemo-photothermal Therapy Promoting Immunogenic Cell Death Based on NIR-II Light-responsive Drug Delivery Systems

Lifeng Hang (hanglf@ustc.edu.cn)
Guangdong Second Provincial General Hospital https://orcid.org/0000-0003-3228-2375
Wuming Li
Guangdong Second Provincial General Hospital
Dandan Men
Jiangxi Science and Technology Normal University
Hua Wen
Guangdong Second Provincial General Hospital
Xinfeng Tang
USTC: University of Science and Technology of China
Chunze Zhou
USTC: University of Science and Technology of China
Xiaofen Ma
Guangdong Second Provincial General Hospital
Guihua Jiang
Guangdong Second Provincial General Hospital

Research

Keywords: Nanocarrier-based drug delivery systems, hollow copper sulfide nanoparticles, doxorubicin, chemo-photothermal therapy, immunogenic cell death

Posted Date: August 6th, 2021

DOI: https://doi.org/10.21203/rs.3.rs-770161/v1

Chemo-photothermal therapy promoting immunogenic cell death based on NIR-II light-responsive drug delivery systems

Lifeng Hang[1*#], Wuming Li[1#], Dandan Men[2#], Hua Wen[1], Xinfeng Tang[3], Chunze Zhou[4], Xiaofen Ma[1], Guihua Jiang[1,*]

[1] *The Department of Medical Imaging, Guangdong Second Provincial General Hospital, Guangzhou, 518037, P. R. China*

[2] *Jiangxi Key Laboratory of Surface Engineering, Jiangxi Science and Technology Normal University, Nanchang, 330013, P. R. China*

[3] *Division of Molecular Medicine, Hefei National Laboratory for Physical Sciences at Microscale, the CAS Key Laboratory of Innate Immunity and Chronic Disease, School of Life Sciences, University of Science and Technology of China, Hefei, 230001, P. R. China*

[4] *Interventional Radiology Department, The First Affiliated Hospital of USTC, Division of Life Sciences and Medicine, University of Science and Technology of China, Hefei 230001, P. R. China*

[#] These authors contributed equally to this work.

***Corresponding author:**

Lifeng Hang, E-mail address: hanglf@ustc.edu.cn

Guihua Jiang, E-mail address: jianggh@gd2h.org.cn

Abstract

Background: Several recent studies have well demonstrated that the chemotherapy or near-infrared-II (NIR-II) photothermal therapy (PTT) can induce immunogenic cell death (ICD). However, single treatment based on the independent chemotherapy or PTT to induce ICD may require high dose of drug, high laser power, or high temperature, which limits their clinical application. We hypothesize that combination of chemotherapy and NIR-II PTT possesses great promise to overcome respective limitations. This manuscript describes the development of polyethylene glycol (PEG) modified hollow Cu_xS nanoparticles (NPs) for synergistic chemo-photothermal therapy to effectively promote ICD.

Results: Hollow structure Cu_xS-PEG NPs were prepared under mild condition by using Cu_2O NPs as sacrificial templates. Cu_xS loaded with doxorubicin (Dox) as NDDSs were characterized for hydrate particle size and surface charge. The morphology, photothermal effect, drug loading/releasing abilities, synergistic chemo-photothermal therapy, and ICD from synergistic therapy of Cu_xS-PEG NPs have been investigated. The *in vitro* outcomes of ICD and chemo-photothermal therapy were assessed in EMT-6 cells. *In vivo* therapeutic studies and immunoreaction were performed in EMT-6 bearing mice where therapeutic outcomes were assessed by tumor volume, immunohistochemical staining, and expression of $CD8^+$ cytotoxic T-lymphocytes. The Cu_xS-PEG NPs with hollow structure show high drug loading capacity (~255 μg Dox per mg of Cu_xS NPs) and stimuli-responsive drug release triggered by NIR-II laser irradiation. The chemo-photothermal strategy more

effectively induces ICD than that of the single treatment, accompanying with the release of adenosine triphosphate, pre-apoptotic calreticulin, and high mobility group box-1. Finally, the synergistic chemo-photothermal therapy based on the Dox/Cu_xS-PEG NPs promotes $CD8^+$ cytotoxic T-lymphocytes infiltration into tumors and achieves ~98.5% tumor elimination.

Conclusion: Therefore, our study emphasizes that the great potentials of Cu_xS-PEG NPs can be used as NIR-II light-responsive NDDSs for the applications of biomedicine and immunotherapy.

Keywords: Nanocarrier-based drug delivery systems, hollow copper sulfide nanoparticles, doxorubicin, chemo-photothermal therapy, immunogenic cell death

Background

Recently, several studies have well demonstrated that the chemotherapy or photothermal therapy (PTT) in the second near-infrared (NIR-II) window can induce immunogenic cell death (ICD), accompanying with the release of damage-related molecular patterns (DAMPs), which serve as immunostimulatory "danger" signals to elicit T cell activation [1-5]. However, single treatment based on the independent chemotherapy or PTT to induce ICD may require high dose of drug, high laser power, or high temperature, which limits their clinical application [6, 7]. We hypothesize that combination of chemotherapy and NIR-II PTT possesses great promise to overcome respective limitations (*i.e.* requirement of high laser power, high dose of drug, and less efficient therapeutic efficacy, *etc.*) and more effectively induces ICD to minimize damage to healthy tissues. Therefore, rationally designing drug delivery systems for chemo-photothermal therapy and improving ICD efficiency is the key to this study.

Compared to the traditional chemotherapy, nanocarrier-based drug delivery systems (NDDSs) have great prospects for precise cancer therapy due to its higher bioavailability, multifunctionality, and low side effects for non-target tissues [8-13]. In particular, NIR-II light-responsive NDDSs serve as promising modalities to realize the demand of drug release at the target disease site and combination with other therapeutic modes [14-18]. Light has been widely used as an external stimulus to control drug release because of its unique advantages such as safety, minimal cross-reaction, and spatiotemporal precision [19, 20]. In addition, the NIR-II light could penetrate a few inches into tissues deeper than NIR-I or visible light, and

displayed no apparent damage to tissues or cells [21, 22]. Meanwhile, based on the photothermal conversion agents (PTCAs) as NDDSs, NIR-II light can be converted into heat for PTT, thereafter triggering drug release from the nanocarriers through thermal effect. Moreover, PTT is a complementary approach to enhance chemotherapeutic efficiency. Thus, using PTCAs as NIR-II light-responsive NDDSs can effectively combine chemotherapy and PTT, which has potential to promote tumor ICD.

Various PTCAs such as noble metal, carbon materials, metal oxide and metal sulfide NPs have been developed to generate heat efficiently for NIR light-responsive NDDSs [23-29]. For example, noble metal nanoparticles (NPs) (gold nanorods, gold nanoparticle agglomerates, platinum NPs) and drugs have been encapsulated into polymeric micelles to create vectors which allow NIR light-triggered drug release [30-35]. Carbon materials are also able to absorb NIR light and generate heat, and therefore the high temperature controls drug delivery from vectors containing carbon materials [36]. In addition, nanocarriers containing metal sulfide or metal oxide as PTCAs release cargoes through photothermal conversion under NIR laser irradiation [37, 38]. However, the reported NIR light-responsive vectors encapsulating both PTCAs and drugs have some limitations including high cost, relatively low drug loading capacity, premature drug leakage, and complex preparation process, which prevented their further widespread applications. Therefore, development of NIR-II light-responsive NDDSs with high drug loading capacity, low cost, and facile preparation process is demanded.

Among the various NIR-II PTCAs, copper sulfide has an optical absorption band peaking wavelength at NIR-II region caused by the d−d energy band transition of Cu^{2+} ions which is independent of the dielectric constant of the surrounding medium [39]. Further, copper sulfide is much less expensive than other NIR-II PTCAs. Different from embedding PTCAs in nanocarriers, hollow nanostructured copper sulfide which exhibits numerous mesoporous pores and a large specific surface area has great application potential to be used as NIR-II light-responsive NDDSs [40]. Importantly, hollow copper sulfide can be eliminated from the living body by slow dissociation of Cu ion from NPs, indicating low biotoxicity of copper sulfide *in vivo* [41].

In this work, we develop a NIR-II photo-responsive NDDS mediated hollow nanostructured copper sulfide (Cu_xS) with modification of polyethylene glycol-lipoic acid (PEG-LA) for drug delivery, NIR-II PTT, and effectively promoting tumor ICD. As illustrated in **Figure 1A**, the hollow Cu_xS NPs are first prepared through Cu_2O NPs template under mild condition. Then, drug molecules (doxorubicin) are loaded into hollow Cu_xS NPs (Defined as Dox/Cu_xS NPs), resulting in a drug a loading factor as high as ~255 μg Dox per mg of Cu_xS NPs, and the obtained Dox/Cu_xS NPs are subsequently modified with PEG-LA as Dox/Cu_xS-PEG NPs. The Dox/Cu_xS-PEG NPs exhibit a controllable drug release manner triggered by the NIR-II laser irradiation (**Figure 1B**). Moreover, excellent photothermal effect of Dox/Cu_xS-PEG NPs has been demonstrated benefiting from strong NIR-II absorption. By synergistic chemo-photothermal therapy, the Dox/Cu_xS-PEG NPs can effectively induce ICD,

accompanying with the release of DAMPs from dying cancer cells. In addition, we found that DAMPs such as adenosine triphosphate (ATP), pre-apoptotic calreticulin (CRT), and high mobility group box-1 (HMGB-1) in dying cells induced by the chemo-photothermal therapy could simultaneously trigger immune responses (**Figure 1C**). Both *in vitro* and *in vivo* results well demonstrated that such multifunctional nanoplatforms could achieve excellent efficiency for tumor suppression. This work develops a NIR-II light-responsive NDDS based on a single-component hollow Cu_xS NPs for synergistic chemo-photothermal therapy and effectively inducing ICD.

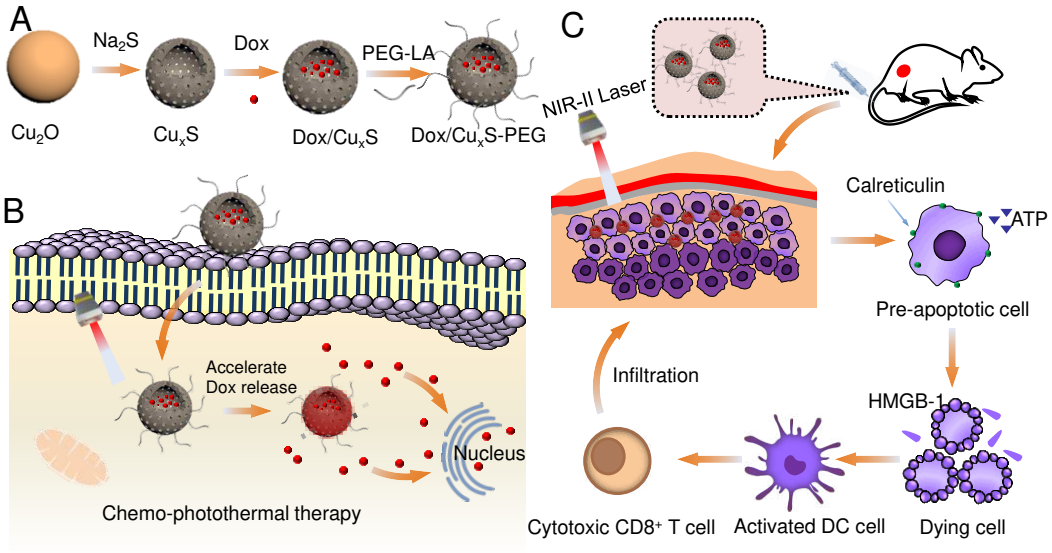

Figure 1. Schematic diagram of the preparation and bio-applications of hollow Cu_xS-PEG NPs. (**A**) The synthesis process of Dox/Cu_xS-PEG NPs. (**B**) The Dox/Cu_xS-PEG NPs for synergistic chemo-photothermal therapy. (**C**) The chemo-photothermal therapy induces ICD accompanying with releasing tumor-associated immunogenic factors which are presented to T cells.

Results and discussion

Preparation and characterizations of Dox/Cu_xS-PEG NPs

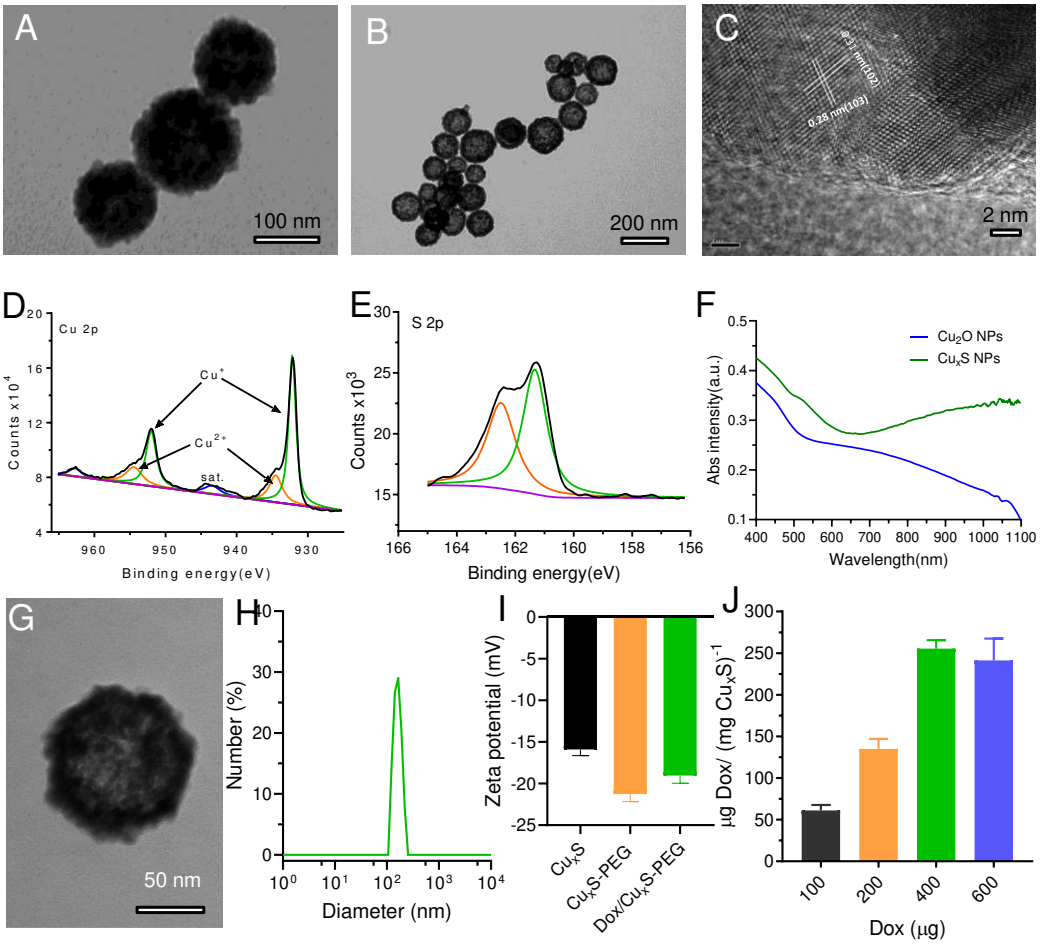

Figure 2. **Characterizations of Dox/Cu_xS-PEG NPs.** Representative transmission electron microscopy (TEM) images of (**A**) Cu_2O nanospheres and (**B**) hollow Cu_xS NPs. (**C**) HRTEM image of hollow Cu_xS NPs. XPS spectra of (**D**) Cu 2p and (**E**) S 2p from Cu_xS NPs. (**F**) UV−Vis−NIR absorption spectra of the Cu_2O nanospheres and hollow Cu_xS NPs. (**G**) The TEM image of hollow Cu_xS-PEG NPs. (**H**) Hydrate particle size of Cu_xS-PEG NPs. (**I**) The Zeta potentials of Cu_xS, Cu_xS-PEG, and Dox/Cu_xS-PEG NPs. (**J**) The Dox loading capacity of per mg of hollow Cu_xS-PEG under different mass of feeding Dox.

Utilizing Cu_2O nanospheres as Cu_xS NPs precursor and template, we report a mild formation of hollow Cu_xS NPs through a facile reduction method in aqueous solution. The precursor Cu_2O nanospheres are synthesized through one-step method, in which PVP is used as the stabilizing agent, copper nitrate as the Cu_xS NPs precursor, and

ethylene glycol (EG) and deionized water as the reaction solvent. Typical transmission electron microscopy (TEM) images (**Figure 2A**) reveal that the Cu_2O nanospheres are spherical NPs with narrow size distribution (**Figure S1**) and average size about ~ 123 nm. To obtain hollow Cu_xS NPs, the Cu_2O nanospheres as the sacrificial templates react with Na_2S solution dropwise under vigorous stirring. Upon the addition, Na_2S continuously etched Cu_2O to fabricate hollow nanostructure immediately meanwhile the porous channels in the resultant NPs, which has the potential for loading drugs. Representative TEM and scanning electron microscopy (SEM) images (**Figure 2B** and **Figure S2**) reveal spherical hollow nanostructure with narrow size distribution (**Figure S3**) and average diameter about ~ 125 nm. To further characterize the hollow Cu_xS NPs, the high-resolution transmission electron microscopy (HRTEM) image (**Figure 2C**) shows that the lattice fringes corresponding to the (103) and (102) plane of Cu_xS crystal, indicating that the obtained hollow NPs is Cu_xS. In addition, the powder X-ray diffraction (PXRD) patterns (Figure S4) of hollow NPs verifies that the all diffraction peaks are assigned to the Cu_xS crystal (PDF#41-0959) [42]. Next, the high-resolution X-ray photoelectron spectroscopy (XPS) spectrum of Cu 2p exhibit Cu element in NPs possessed Cu^+ and Cu^{2+} (**Figure 2D**), and S element is S^{2-} state (**Figure 2E**) [43]. Furthermore, the corresponding UV-vis-NIR spectrum (**Figure 2F**) of hollow Cu_xS NPs showed the optical absorption band peaking wavelength at NIR region (range from NIR-I to NIR-II), which displayed the potential for the NIR-II phototherapy. These results well demonstrated that we successfully achieved hollow Cu_xS NPs with absorption at NIR-II region.

To improve the biocompatibility of Dox/Cu_xS NPs, PEG-LA due to good biocompatibility and long-term circulation is used to modify the hollow NPs based on the Cu-S bond. The typical TEM image (**Figure 2G**) displays the observed faint dense corona surrounding the surface of Cu_xS NPs, demonstrating that a uniform PEG layer is coated on the hollow Cu_xS NPs (Cu_xS-PEG). The average hydrodynamic size of Cu_xS-PEG NP is ~ 120 nm (**Figure 2H**), consistent with that of the Cu_2O templates. Therefore, the hollow Cu_xS NPs have great potential to loading with antitumor drugs for chemotherapy, and we select Dox molecules as a model drug to evaluate their capacity. Meanwhile, the Zeta potential of Cu_xS-PEG NPs with strong negative charge (–21.2 mV) is higher than than that of the pristine Cu_xS NPs (–15.9 mV) (**Figure 2I**). After loaded with positively charged Dox, the Zeta potential of Dox/Cu_xS-PEG NPs decreases to –19.3 mV, indicating the successful Dox loading in NPs. Then, the loading capacity of Dox was measured by UV-vis spectra according to the standard line relation between concentration and absorption intensity (**Figure S5**). The UV-vis spectra of feeding Dox in solution and supernatant were respectively recorded (Figure S6), and the maximum loading capacity of Dox in hollow Cu_xS NPs is quantified to be ~ 255 μg Dox per mg of NPs (**Figure 2J**).

Properties of Cu_xS-PEG NPs for drug releasing and in vitro chemo-photothermal therapy

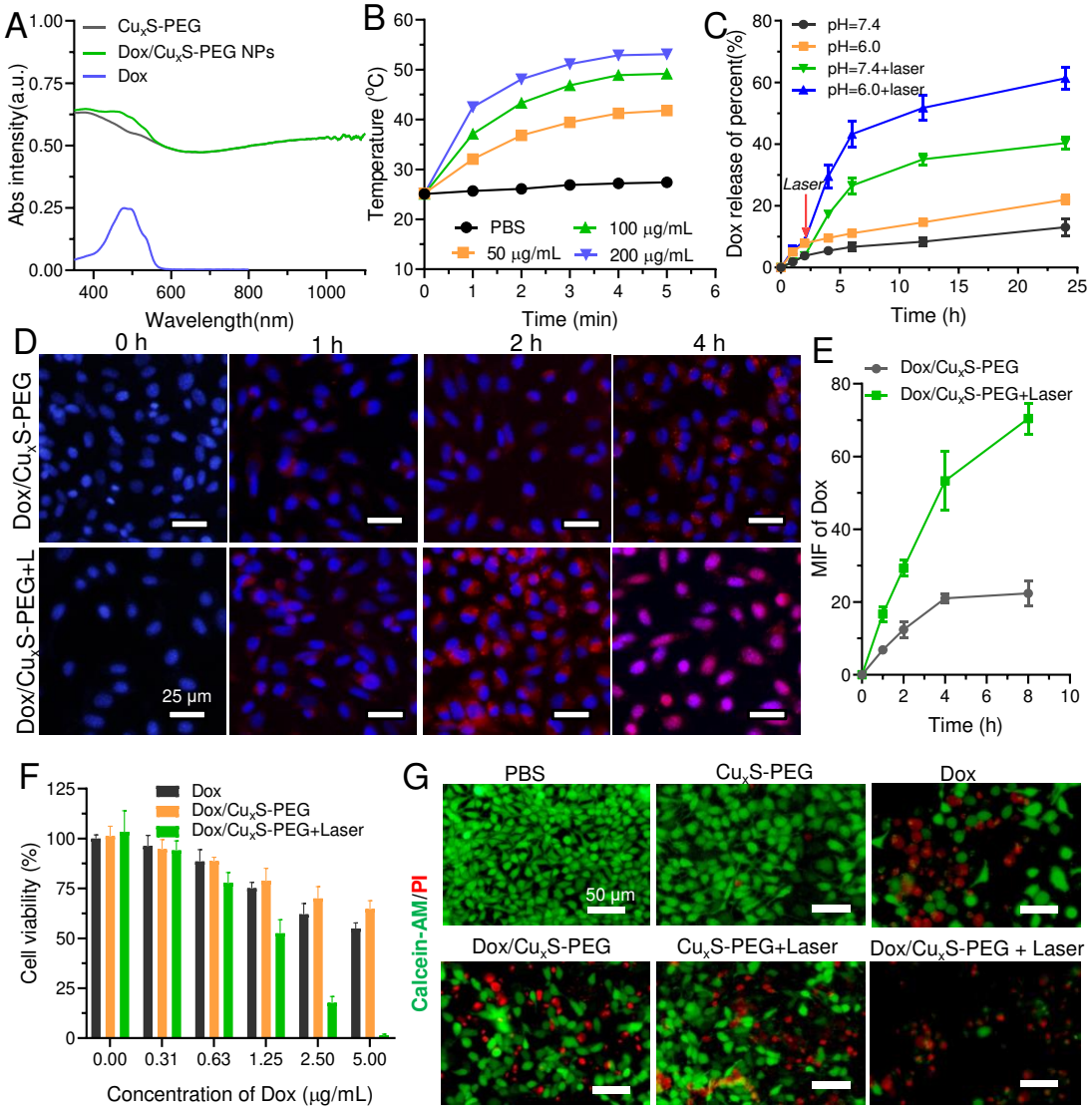

Figure 3. Drug releasing and in vitro chemo-photothermal therapy of Dox/Cu$_x$S-PEG NPs. (**A**) The UV-vis-NIR spectra of Cu$_x$S-PEG NPs, Dox/Cu$_x$S-PEG NPs, and Dox. (**B**) The photothermal conversion curves of Cu$_x$S-PEG NPs dispersions with different concentrations (0, 50, 100, and 200 μg·mL^{-1}). The dispersions are irradiated with a 1064 nm laser (1.0 W·cm^{-2}). (**C**) Dox release performance at pH = 6.0 and 7.4 with or without laser irradiation (1.0 W·cm^{-2}). (**D**) Fluorescence images of EMT-6 cells after treated with Dox/Cu$_x$S-PEG NPs and Dox/Cu$_x$S-PEG NPs plus NIR-II laser, respectively. The red and blue signals represent the Dox fluorescence and DAPI-stained cell nuclei, respectively. (**E**) MIF of Dox in the cell at different time point. (**F**) Cell viability of EMT-6 cells after treated with free Dox, Dox/Cu$_x$S-PEG NPs and Dox/Cu$_x$S-PEG NPs plus NIR-II laser. (**G**) Propidium iodide (PI) and Calcein-AM staining of the EMT-6 cells after administration with different groups: PBS, Cu$_x$S-PEG NPs, Dox, Dox/Cu$_x$S-PEG NPs, Cu$_x$S-PEG NPs plus laser, and Dox/Cu$_x$S-PEG NPs plus laser, was measured by fluorescence microscope.

Compared with the absorption spectrum of the hollow Cu_xS-PEG NPs, absorption spectrum of Dox/CuxS-PEG NPs shows a wide peak in the range of 380~600 nm, which is derived from the encapsulated Dox molecules (**Figure 3A**), further indicaiting the successful Dox loading in NPs. Next, the photothermal conversion performance of hollow Cu_xS-PEG NPs was studied by irradiating the Cu_xS-PEG NPs aqueous dispersions with 1064 nm laser (1.0 $W \cdot cm^{-2}$) under different concentration (0, 50, 100, and 200 $\mu g \cdot mL^{-1}$). The recorded temperature change curves of hollow Cu_xS-PEG NPs in PBS solution rapidly increases within 4 min, and then reached to a plateau. When the NPs concentrations increases from 50 to 200 $\mu g \cdot mL^{-1}$, the temperature change (ΔT) is 16.6, 24.1, and 27.9 ^{o}C (**Figure 3B**), respectively. In stark contrast, the temperature of PBS solution shows negligible temperature increase (~2.3 °C) under same conditions. Then, the photothermal stability of Cu_xS-PEG NPs (50 $\mu g \cdot mL^{-1}$) is investigated by repeatedly irradiating aqueous dispersions for four ON/OFF cycles. No significant reduction was observed over the four cycles (**Figure S7**), suggesting that the Cu_xS NPs are photothermal stability for the NIR-II PTT. Therefore, the hollow Cu_xS NPs can be used for NIR-II PTT for triggering drug releasing.

The Dox releasing behavior was studied in PBS solutions (Dox/Cu_xS NPs: 100 $\mu g \cdot mL^{-1}$) at different pH (6.0 and 7.4) with or without laser irradiation (1.0 $W \cdot cm^{-2}$) for 3 min. Under the slightly acidic condition (pH = 6.0), Dox release rate is faintly faster than that of under neutral conditions (pH = 7.4). At pH 6.0 after 24 h, the released Dox amount reached to 22% which is higher than that at pH = 7.4 (~13.1%)

(**Figure 3C**), deriving from the increased hydrophilia and protonation of Dox under acid environment. In addition, a explosive release of Dox observed under laser irradiation due to the rapid local temperature increase which can accelerate Dox dissolution from the NPs. Moreover, accumulated Dox amount in acidic and neutral environment under laser irradiation after 12 h is respectively almost 3.5-fold (51.7% vs 14.6%) and 4.1-fold (35.1% vs 8.4%) as that without irradiation. Therefore, hollow Cu_xS NPs can be used as NIR-II light-responsive NDDSs for on-demand drug delivery.

Before evaluating the behavior of intracellular drug delivery, the endocytosis and cytotoxicity of hollow Cu_xS-PEG NPs have been measured by the inductively coupled plasma mass spectrometry (ICP-MS) and MTT assay, respectively. Firstly, Cu_xS-PEG NPs (50 and 100 $\mu g \cdot mL^{-1}$) are incubated with EMT-6 cells for different time (1, 2, 4, and 6 h), and the concentration and incubation time-dependent phenomena are observed (**Figure S8**). Next, the cytotoxicity of Cu_xS-PEG NPs was measured with various concentrations (ranging from 0~100 $\mu g \cdot mL^{-1}$) incubated with EMT-6 cells for 48 h. The MTT assay results show that the cell survival rate remains above 93% when the concentration of Cu_xS-PEG NPs is increased to 100 $\mu g \cdot mL^{-1}$ (**Figure S9**), indicating that the Cu_xS-PEG NPs have no significant cytotoxicity to EMT-6 cells at the tested concentrations. Then, the intracellular conversion performance of Cu_xS-PEG NPs is investigated on EMT-6 cells after incubating with NPs (50 $\mu g \cdot mL^{-1}$) for 4 h, and the temperature of cells increases to 43.8 ^{o}C under irradiation with 1064 nm laser (1.0 $W \cdot cm^{-2}$) (**Figure S10**). After incubating with Cu_xS-PEG NPs for 4 h,

EMT-6 cells viabilities gradually decrease with increasing concentrations of NPs after irradiation with 1064 nm laser for 10 min (1.0 $W \cdot cm^{-2}$), remaining only approximately 85%, 69.7% and 54.9% at concentration of 25, 50 and 100 $\mu g \cdot mL^{-1}$, respectively. Therefore, the Cu_xS-PEG NPs can be used as NIR-II PTCAs for PTT.

The drug delivery in cells was tested by incubating Dox/Cu_xS-PEG NPs with EMT-6 cells for different time (0, 1, 2, and 4 h) irradation with or without laser, followed stained by 4′,6-diamidino-2-phenylindole (DAPI). The fluorescence signals of Dox are observed in EMT-6 cells treated with Dox/Cu_xS-PEG NPs at different time points (**Figure 3D**). In addition, the fluorescence intensity of Dox increases obviously in the cells after treating with Dox/Cu_xS-PEG NPs plus laser, indicating that the NIR-II light can accelerate the release of Dox. As shown in Figure 3E, the mean fluorescence intensity (MFI) of Dox is quantified from images (Figure 3D), which was consistent with results in **Figure 3C**. Therefore, these results have well demonstrated that Cu_xS-PEG NPs can be used as NIR-II light-responsive NDDSs for drug delivery in cells.

Next, the NIR-II light-responsive performance of Dox/Cu_xS-PEG NPs for synergistic chemo-photothermal therapy is studied. EMT-6 cells are treated by free Dox (chemotherapy), Dox/Cu_xS-PEG NPs (chemotherapy), or Dox/Cu_xS-PEG NPs plus laser (chemo-photothermal therapy) for cell viability measurement (Figure 3F). At test concentration, the Dox/Cu_xS-PEG NPs plus laser group shows stronger killing effects than other group. For example, at 5 $\mu g \cdot mL^{-1}$ of Dox, chemo-photothermal therapy killed ~98.7% cancer cells, much higher than either free Dox (~46.1%) and

Dox/Cu_xS-PEG NPs (~36.3%). Herein, dead/live staining measurement is employed to test the chemo-photothermal therapy effect of Dox/Cu_xS-PEG NPs on the cancer cells. Six groups including PBS, Cu_xS-PEG NPs, Dox, Dox/Cu_xS-PEG NPs, Cu_xS-PEG NPs plus laser, Dox/Cu_xS-PEG NPs plus laser are administrated on the EMT-6 cells. As presented in **Figure 3G**, almost no cells die (green fluorescence) in groups PBS and Cu_xS-PEG NPs indicating the no significant cytotoxicity of Cu_xS-PEG NPs, while the number of dead cells (red fluorescence) with treatment of Dox/Cu_xS-PEG NPs plus laser significantly increases. Therefore, the synergistic chemo-photothermal therapy of Dox/Cu_xS-PEG NPs plus laser displays superior antitumor effect triggered by the NIR-II light.

Detection of DAMPs released from the dying cells

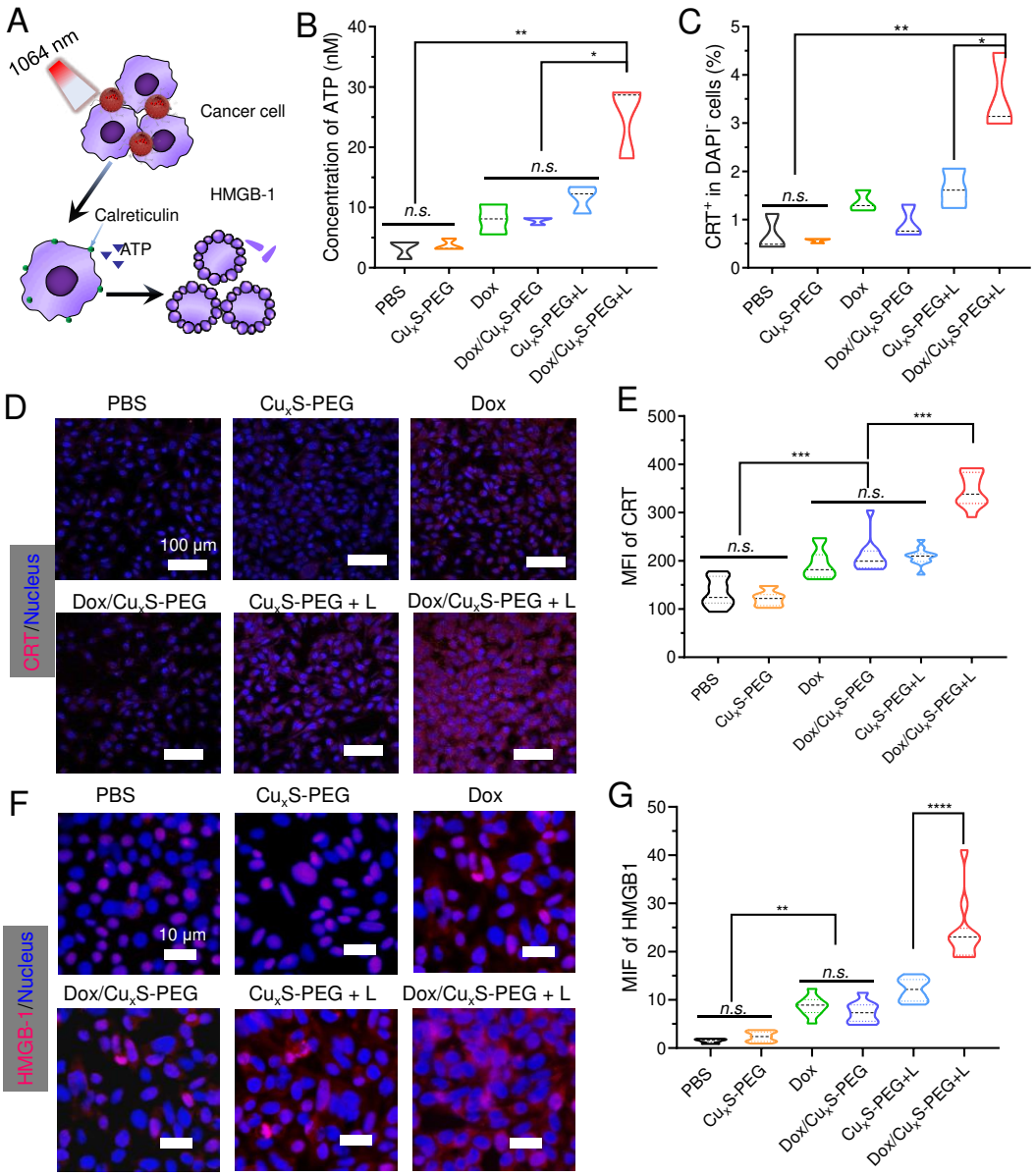

Figure 4. DAMPs released from the dying cells with chemo-photothermal treatment. (**A**) Schematic illustration of ICD induced by the chemo-photothermal therapy. (**B**) The concentration of ATP releasing from the EMT-6 cells treated with different groups. (**C**) Cell-surface exposure of calreticulin (CRT) of $DAPI^-$ EMT-6 cells after administration with different treatments by flow cytometry analysis. (**D**) Immunofluorescence microscopy of CRT expression on the cell surface of EMT-6 cells treated with different groups and measured after immunofluorescence staining scale bar: 100 μm. (**E**) The MIF of CRT from (D). (**F**) HMGB-1 release from cell nucleus to cytoplasm of EMT-6 cells treated with different groups and measured after immunofluorescence staining, scale bar: 10 μm. (**G**) The MIF of released HMGB-1 from (F). Six groups are respectively PBS, Cu_xS-PEG NPs, Dox, Dox/Cu_xS-PEG NPs, Cu_xS-PEG NPs plus laser, and Dox/Cu_xS-PEG NPs plus laser. Data are shown as mean ± standard deviation (n = 3), *p < 0.05, **p < 0.005, ***p < 0.001, and ****p < 0.0001.

To date, ICD has been well demonstrated in the chemotherapy or photothermal therapy. As shown in schematic illustration (**Figure 4A**), DAMPs release from the dying cells after treatment with phototherapy. A "find-me" signal is delivered by the released ATP molecules which cause dendritic cells (DCs) to produce cytokine [44, 45]. In comparison to the groups of PBS, Cu_xS-PEG NPs, Dox, Dox/Cu_xS-PEG NPs, Cu_xS-PEG NPs plus laser, we observe a highest level of extracellular ATP at 25.3 nM after treatment with the synergistic chemo-photothermal therapy by using a luciferase-based probe (**Figure 4B**). Moreover, CRT exposure is a mediator of tumor immunogenicity and potent "eat-me" signal [46]. Flow cytometry measurement reveals that the CRT is most highly expressed after treatment with Dox/Cu_xS-PEG NPs under 1064 nm laser irritation, indicating that combination chemotherapy and PTT can more effectively induce the CRT exposure (**Figure 4C**). The direct fluorescence microscopy observation (**Figure 4D**) and MIF of CRT from fluorescence image (**Figure 4E**) further confirm the most significant exposure of CRT after treatment with synergistic chemo-photothermal therapy. To the best of our knowledge, HMGB-1 releasing from cell nucleus in dying cells can trigger inflammation, attract various immune cells and cause DC maturation [47]. In our work, we observe that the treatment of Dox/Cu_xS-PEG NPs plus 1064 nm laser also shows a most significant increase of the translocation of HMGB-1 from nuclei to extracellular space (**Figure 4F**). The MIF of HMGB-1 in extracellular space from Figure 4F indicates synergistic chemo-photothermal therapy can effectively promote the release of HMGB-1 (**Figure 4G**).

Next, *in vitro* DCs maturation was investigated using Bone marrow-derived dendritic cells (BMDCs). After treated with PBS, Cu_xS-PEG NPs, Dox, Dox/Cu_xS-PEG NPs, Cu_xS-PEG NPs plus laser, and Dox/CuxS-PEG NPs plus laser, the harvested dying EMT-6 cells were incubated with BMDCs for 10 h at 37 ^oC and measured by flow cytometry. A significant percentage of DCs maturation (38.2%) is found in the BMDCs incubated with Dox/Cu_xS-PEG NPs plus laser pre-treated cancer cells (**Figure S11**), which is higher than that of PBS (11.9%), Cu_xS-PEG NPs (12.4%), Dox (24.1%), Dox/Cu_xS-PEG NPs (23.7%), and Cu_xS-PEG NPs plus laser (28.3%). Therefore, the combination of chemotherapy and PTT can more effectively generate DAMPs in dying cells and benefit the DCs maturation.

The *in vivo* chemo-photothermal therapy and ICD

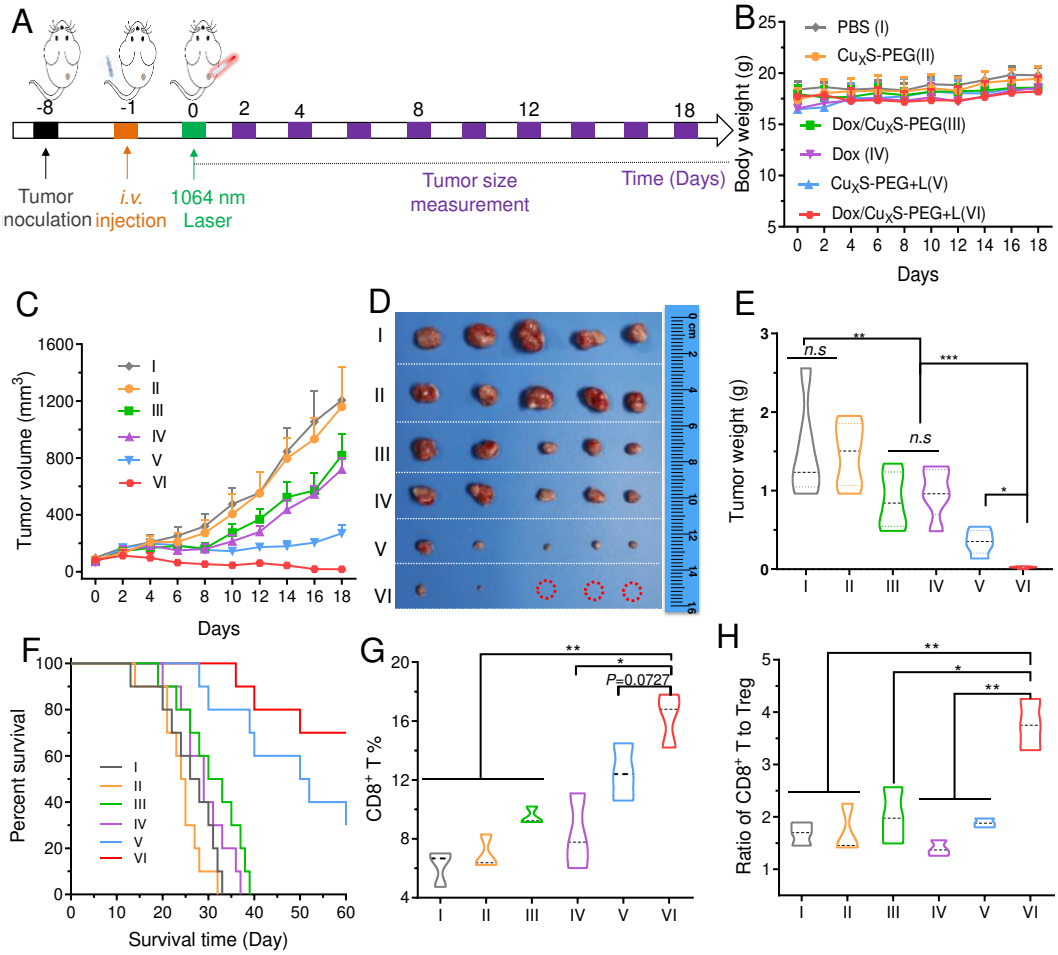

Figure 5. ***In vivo*** **chemo-photothermal therapy and ICD**. (**A**) Schematic illustration showing the treatment regimen, EMT-6 cells inoculation in the flank of the mouse. The mice (n = 5) received different treatments and irradiated with NIR-II laser for 10 min (1 W·cm^{-2}). (**B**) Mouse body weight, (**C**) Tumor growth curve, (**D**) photographs of tumor, (**E**) Tumor weight of different groups: PBS (I), Cu_xS-PEG NPs (II), Dox/Cu_xS-PEG NPs (III), Dox (IV), Cu_xS-PEG NPs plus laser (V), and Dox/Cu_xS-PEG NPs plus laser (VI). (**F**) Morbidity-free survival of different groups of mice with EMT-6 tumors after various treatments. After NIR-II photo-treatments for 3 days, percentage of anti-tumor CD8$^+$ cytotoxic T-lymphocytes cells among leukocytes (**G**) and CD8$^+$ T cells to Tregs in tumors (**H**) were analyzed by flow cytometry analysis. Data are shown as mean ± standard deviation *p < 0.05, **p < 0.005, ***p < 0.001.

Inspired by the attractive *in vitro* results, we finally verify the antitumor efficacy *in vivo* by chemo-photothermal therapy. Before evaluation, we first assessed the pharmacokinetics of Cu_xS-PEG NPs (10 mg·kg^{-1}) by intravenously injecting to tumor-bearing mice (n = 3). Then, 20 μL of blood sample was obtained at

pre-determined time points (0, 1, 2, 4, 6, 12, 24, and 48 h), and ICP-MS analysis displayed that the Cu_xS-PEG NPs possessed long-term circulation *in vivo* (**Figure S12**), owing to the modification of PEG on the surface of NPs. Next, we investigate the biodistributions of Cu_xS-PEG NPs in the major tissues including heart, liver, spleen, lung, kidney and tumor. The mice were sacrificed at different time (12, 24, and 48 h) after adimistration of Cu_xS-PEG NPs, and all collected tissues were treated with chloroazotic acid. The ICP-MS measurement indicates that the concentrations of Cu_xS-PEG NPs in the tumor sites are ~4.3%, ~7.8% and ~6.7% at 12, 24, and 48 h, respectively (**Figure S13**). Therefore, the time-point at 24 h after intravenous injection of NPs is suitable for *in vivo* experiments. To verify *in vivo* photothermal conversion properties of Cu_xS-PEG NPs, the typical thermal images of mice under irradiation with the 1064 nm laser were recorded by the infrared camera (**Figure S14**). The temperature at tumor sites with the treatments of Cu_xS-PEG NPs plus laser increases to 45.06 ^{o}C within 5 min (**Figure S15**), while the temperature of PBS group is silghtly increased. These results reveal that the enhanced permeability and retention (EPR) effect induced Cu_xS-PEG NPs accumulating into the the tumor sites passively.

Next, we investigate the antitumor efficacy of the synergistic chemo-photothermal therapy based on the Cu_xS-PEG NPs triggered by NIR-II laser. As the schematic illustration shown in the Figure 5A, when the tumors were growing to ~ 100 mm^3, six groups (n = 5) of the EMT-6 tumor bearing mice were received different treatments as follows: (I) PBS as control, (II) Cu_xS-PEG NPs (dose of 10 $mg \cdot kg^{-1}$), (III) Dox/Cu_xS-PEG NPs, (IV) only Dox, (V) Cu_xS-PEG NPs plus laser,

and (VI) Dox/Cu_xS-PEG NPs plus laser (1 $W \cdot cm^{-2}$ for 10 min). Subsequently, the mice weight and tumor volume were monitored every two days. The body weight of mice in all groups shows no remarkable undulation during the therapeutic process (**Figure 5B**), which indicates the security of NIR(II)-induced synergistic chemo-photothermal therapy. Moreover, the groups (V) and (VI) efficiently inhibite tumor growth by ~76.8% and ~98.5% respectively, after irradiation treatment with 1064 nm laser (**Figure 5C**). Meanwhile, on the 18th day after the first treatments, the the photos (**Figure 5D**) and weight measurement (**Figure 5E**) of the excised tumors from sacrificial mice of all groups verify that Dox/Cu_xS-PEG NPs plus laser group can realize more efficient tumor suppression than either PTT or chemotherapy alone, which is consistent with cellular reuslts. Remarkably, all the tumors in Dox/Cu_xS-PEG NPs plus laser group (VI) are alomst completely eliminated at the end of therapy (**Figure S16**). In contrast, the groups (I) and (II) show negligible influence on the tumor growth, and slight inhibition effect is observed in Dox/Cu_xS-PEG NPs and Dox groups. To assess the therapeutic effect, the excised tumors were sliced and stained with H&E (**Figure S17**) and TUNEL staining (**Figure S18**), which demonstrated that Group VI displayed much severer necrosis of tumor cells than the other groups. To further evaluate the therapeutic outcomes of Dox/Cu_xS-PEG NPs plus laser based on chemo-photothermal therapy, the survival experiment was carried out on the EMT-6 tumors bearing mice after treated with different groups. We find that seven of ten tumors bearing mice can survive for 60 days after treated Dox/Cu_xS-PEG NPs plus laser, in marked contrast to mice in the PBS, Cu_xS-PEG NPs,

Dox/CuxS-PEG NPs, and only Dox groups in which all die within 30-40 days (Figure 5F). These experimental results indicate that the breast cancer could be effectively inhibited by chemo-photothermal therapy.

Next, we aslo investigated the immune response from ICD after treatments with chemo-photothermal therapy, which can trigger cytotoxic T-lymphocytes and induce anti-tumor immunity [48]. In our experiments, the EMT-6 tumor bearing mice were divided into six groups (n = 5) and administrated with different treatments including PBS (I), Cu_xS-PEG NPs (II), Dox/Cu_xS-PEG NPs (III), Dox (IV), Cu_xS-PEG NPs plus laser (V), and Dox/Cu_xS-PEG NPs plus laser (VI). At 72 h after treatments with different groups, the PBS and Cu_xS-PEG NPs with *i.v.* injection alone failed to promote $CD8^+$ cytotoxic T-lymphocytes infiltration into tumors. On the contrary, the percentage of $CD8^+$ cytotoxic T-lymphocytes in tumors of mice after the Dox/Cu_xS-PEG NPs plus laser significantly increases to ~16.3%, which is higher than that in Dox (~8.3%) and Cu_xS-PEG NPs plus laser (~12.5 %) (**Figure 5G**). The regulatory T cells (Tregs) can hamper effective anti-tumor immune responses. It is found that the Dox/Cu_xS-PEG NPs based chemo-photothermal therapy can significantly reduce the percentages of Tregs in the tumors (**Figure S19**). Therefore, both $CD8^+$/Treg ratio are greatly enhanced in tumors after the treatment of Dox/Cu_xS-PEG NPs based chemo-photothermal therapy (**Figure 5H**). From the abovementioned results, the Dox/Cu_xS-PEG NPs based chemo-photothermal therapy can more effectively induce ICD to elicit an adaptive immune response.

Conclusion

In summary, we successfully develop a hollow structure Cu_xS-PEG NPs for NIR-II light-responsive drug delivery and synergistic chemo-photothermal cancer therapy, which can effectively induce ICD. The Dox moleculars can be loaded into the Cu_xS-PEG NPs, displaying a controllable drug release triggered by NIR-II laser irradiation. The synergistic chemo-photothermal strategy cab more effectively trigger ICD than that of single treatment. *In vitro* and *in vivo* results demonstrated that the synergistic chemo-photothermal therapeutic efficacy based on the Dox/Cu_xS-PEG NPs is superior to that of monotherapy. Additionally, the synergistic chemo-photothermal therapy can promote $CD8^+$ cytotoxic T-lymphocytes infiltration into tumours, which will provide an effective approach to accomplish a photo-immunological response and elicit effective anti-tumor immunotherapy. Such Cu_xS-PEG NPs may encourages the development of NIR-II light-responsive NDDSs for further biomedical utility.

Methods

Materials

$Cu(NO_3)_2$, Polyvinylpyrrolidone (PVP, K30), hydrazine hydrate, dimethylsulfoxide, sodium sulphide (Na_2S), doxorubicin hydrochloride, methylene chloride, diethyl ether, 3-(4,5-dimethylthiazol-2-yl)-2,5-diphenyltetrazolium bromide (MTT), glycol, 4′,6-diamidino-2-phenylindole (DAPI), lipoic acid, polyethylene glycol (PEG_{5k}), 1-(3-Dimethylaminopropyl)-3-ethylcarbodiimide hydrochloride (EDC), and 4-dimethylaminopyridine (DMAP) were all purchased from Aladdin reagent Co. LTD. Dulbecco's modified eagle medium (DMEM) and Fetal bovine serum (FBS) were bought from Gibco BRL (Eggenstein, Germany). Deionized water (~18.2 MΩ·cm) obtained from a Milli-Q Water Purification System was used in all the experiments.

Synthesis of hollow Cu_xS nanospheres

First, 50 mg $Cu(NO_3)_2$ and 1 g PVP were added into a mixture of 50 mL deionized water and glycol (V:V=1:1) to form homogeneous solution under vigorous stirring. Then, hydrazine hydrate (30 μL) was immediately added into the above solution keeping stirring for 5 min. Subsequently, the Cu_2O NPs were collected by centrifugation and washed several times with deionized water.

Next, the obtained Cu_2O NPs were resuspended in the 10 mL of DI water, and 1 mL Na_2S aqueous solution (0.5 M) was introduced into Cu_2O NPs suspension keeping stirring for 30 min to prepare hollow Cu_xS NPs. Finally, the Cu_xS NPs was harvested by centrifugation and washed several times with deionized water.

Synthesis of Cu_xS-PEG NPs

The LA-PEG was prepared according to our previous report [49]. Typically, 5 g $mPEG_{5k}$ was dissolved in 20 mL dichloromethane. After fully dissolved, lipoic acid (1.0 g), EDC (1.0 g), and DMAP (0.4 g) were introuduced in 20 mL of dichloromethane and activated in an ice bath for 3 h. The mixture further reacted for 72 h, and then the products were precipitated with diethyl ether for three times and dried overnight in vacuo to obtain LA-PEG.

Next, the hollow Cu_xS NPs were incubated with LA-PEG solution (10 $mg \cdot mL^{-1}$) for 24 h in room, and the Cu_xS-PEG NPs were collected by centrifugation to remove redundant LA-PEG.

Study of the NIR-II photothermal effect

To explore the photothermal conversion effect of the synthesized Cu_xS-PEG NPs dispersion containing different concentrations (0, 50, 100, and 200 $\mu g \cdot mL^{-1}$) were irradiated by a 1064 nm laser (Xi'an Minghui Optoelectronic Technology) at a power density of 1 $W \cdot cm^{-2}$ for 5 min. The temperature at each time point was recorded by the NIR thermal imaging camera (IC17320, Infrared Camera Inc).

The photothermal stability of Cu_xS-PEG NPs (50 $\mu g \cdot mL^{-1}$) was measured by irradiating with a 1064 nm laser (1.0 $W \cdot cm^{-2}$) for 3 min, followed by shuting off laser for 3 min. The laser was applied to on/off with an interval of 3 min for four cycles.

To further evaluate the photothermal response of Cu_xS-PEG NPs in cells, EMT-6 cells were incubated with Cu_xS-PEG NPs (50 $\mu g \cdot mL^{-1}$) in DMEM for four hours. Then the collected cells were irradiated by a 1064 nm laser (1.0 $W \cdot cm^{-2}$) for 10 min. Meanwhile, the photothermal heating curves were recorded by the NIR thermal

imaging camera.

EMT-6 tumor-bearing mice were respectively intravenously injected with Cu_xS-PEG NPs (10 $mg \cdot kg^{-1}$) and PBS (as control group). After 24 hours, all mice were irradiated with a 1064 nm laser (1 $W \cdot cm^{-2}$) for 6 min in the tumor site. The thermal images and temperature at tumor site were recorded simultaneously with infrared thermal camera.

Drug loading and releasing experiments

Typically, different amount of Dox was mixed with Cu_xS NPs (1 $mg \cdot mL^{-1}$) dispersion in PBS under stirring at ambient temperature for 24 h, followed by the addition of the LA-PEG solution (10 $mg \cdot mL^{-1}$) for further incubating for 24 h. The Dox-loaded Dox/Cu_xS-PEG NPs were obtianed by centrifugation to discard the unencapsulated Dox and excess PEG in the supernatant. To evaluate the drug loading capacity of Cu_xS-PEG NPs, the supernatant after centrifugation was carefully collected for the UV-Vis spectrum measurement. The Dox loading capacity was calculated corresponding to standard calibration curve.

For the stimuli-responsive Dox release study, Dox/Cu_xS-PEG NPs dispersions (200 $\mu g \cdot mL^{-1}$) with pH = 6.0 and 7.4 with or without irradiation of NIR-II laser were tested at selected time points (*i.e.*, 0, 1, 2, 4, 6, 12, and 24 h).

To study the intracellular drug delivery of the Dox/Cu_xS-PEG NPs, EMT-6 cells were incubated with Dox/Cu_xS-PEG NPs dispersion for 0, 1, 2, and 4 h with or without 5 min NIR-II laser irradiation. After the treatments, the cells were measured by the inverted fluorescence microscope for different time point.

In Vitro chemotherapy and chemo-photothermal therapy

To study the chemotherapy and chemo-photothermal effect of the Dox/Cu_xS-PEG NPs in cancer cells, EMT-6 cells (3×10^3) were seeded in 96-well plate and treated with the free Dox, Dox/Cu_xS-PEG, and Dox/Cu_xS-PEG + laser, respectively. The concentration of free Dox was normalized to be equivalent to the loaded Dox in the Cu_xS-PEG NPs. After the treatments, the cell viability of cancer cells was measured by MTT assay.

In vivo chemo-photothermal therapy

When the tumor volumes were about 100 mm^3, the mice were randomly divided into the following six groups (n = 5): (I) Control (PBS), (II) Cu_xS-PEG NPs, (III) Dox/Cu_xS-PEG NPs, (IV) free Dox only, (V) Cu_xS-PEG NPs + Laser, and (VI) Dox/Cu_xS-PEG NPs + Laser. After tail intravenous injection with free Dox, Cu_xS-PEG NPs and Dox/Cu_xS-PEG NPs dispersions, the mice in group (V) and (VI) were exposed to 1064 nm laser (1.0 $W \cdot cm^{-2}$) for 10 min. During the irradiation, the tumor temperature was monitored by the IR thermal camera. After laser irradiation, the tumor length and width of the mice were measured every 2 days. The tumor volume was calculated according to the following formula: (tumor volume) = (length) $\times$ $(width)^2/2$. At the end of experiment, the tumor tissues were excised and weighed. Finally, the harvested tumor tissues were fixed in the paraformaldehyde solution, and then the paraffin-embedded tumors were sectioned for the hematoxylin and eosin (H&E) and terminal deoxynucleotidyl transferase mediated dUTP nick-end labeling (TUNEL) staining staining before the observation under a fluorescence microscope.

List of abbreviations

PTT: photothermal therapy; **ICD**: immunogenic cell death; **DAMPs**: damage-related molecular patterns; **NDDSs**: nanocarrier-based drug delivery systems; **PTCAs**: photothermal conversion agents; **NPs**: nanoparticles; **Dox**: doxorubicin; ATP: adenosine triphosphate; **CRT**: calreticulin; **HMGB-1**: high mobility group box-1; **PEG-LA**: glycol-lipoic acid; **TEM**: transmission electron microscopy; **SEM**: scanning electron microscopy; **PXRD**: powder X-ray diffraction; **MFI**: mean fluorescence intensity; **DCs**: dendritic cells; **ICP-MS**: inductively coupled plasma mass spectrometry; **H&E**: hematoxylin and eosin; **TUNEL**: terminal deoxynucleotidyl transferase mediated dUTP nick-end labeling.

Declarations

Ethics approval and consent to participate

All animals received were cared in compliance with the guidelines outlined in the Guide for the Care and Use of Laboratory Animals, and all procedures were approved by the Guangdong Second Provincial General Hospital Animal Care and Use Committee.

Availability of data and materials

All data generated or analysed during this study are included in this published article [and its supplementary information files].

Competing Interests

The authors have declared that no competing interest exists.

Funding

This work is supported by the National Natural Science Foundation of China (NSFC) (51903162 and U1903120), Science Foundation of Guangdong Second Provincial General hospital (YN2018-001), Doctoral Workstation of Guangdong Second Provincial (2019BSG2024), Key Research and Development Program of Anhui Province (202004J07020015), and Guangzhou Science and Technology Plan Project (202102020646).

Authors' contributions

L Hang, L Wu and D Men: Methodology, Project administration, Writing - original draft. **H Wen** and **X Tang:** Methodology, Investigation. **C Zhou and X Ma:** Methodology, Visualization. **L Hang and G Jiang:** Writing - review & editing, Validation, Supervision.

Acknowledgements

We thank the staff of the Medical Research Center of Guangdong Second Provincial General Hospital for technical support.

References

[1] Chen Q, Xu L, Liang C, Wang C, Peng R, Liu Z. Photothermal therapy with immune-adjuvant nanoparticles together with checkpoint blockade for effective cancer immunotherapy. Nat Commun. 2016; 7: 1-13.

[2] Lu K, He C, Guo N, Chan C, Ni K, Weichselbaum RR, et al. Chlorin-based nanoscale metal–organic framework systemically rejects colorectal cancers via synergistic photodynamic therapy and checkpoint blockade immunotherapy. J Am Chem Soc. 2016; 138: 12502-10.

[3] Duan X, Chan C, Lin W. Nanoparticle-mediated Immunogenic Cell Death Enables and Potentiates Cancer Immunotherapy. Angew Chem Int Ed. 2019; 58: 670-80.

[4] Wang M, Song J, Zhou F, Hoover AR, Murray C, Zhou B, et al. Nir-triggered

phototherapy and immunotherapy via an antigen-capturing nanoplatform for metastatic cancer treatment. Adv Sci. 2019; 6: 1802157.

[5] Wang C, Xu L, Liang C, Xiang J, Peng R, Liu Z. Immunological responses triggered by photothermal therapy with carbon nanotubes in combination with anti-CTLA-4 therapy to inhibit cancer metastasis. Adv Mater. 2014; 26: 8154-62.

[6] Yu GT, Rao L, Wu H, Yang LL, Bu LL, Deng WW, et al. Myeloid-Derived Suppressor Cell Membrane-Coated Magnetic Nanoparticles for Cancer Theranostics by Inducing Macrophage Polarization and Synergizing Immunogenic Cell Death. Adv Funct Mater. 2018; 28: 1801389.

[7] Song W, Kuang J, Li C-X, Zhang M, Zheng D, Zeng X, et al. Enhanced immunotherapy based on photodynamic therapy for both primary and lung metastasis tumor eradication. ACS Nano. 2018; 12: 1978-89.

[8] Majumder J, Taratula O, Minko T. Nanocarrier-based systems for targeted and site specific therapeutic delivery. Adv Drug Deliver Rev. 2019;144: 57-77.

[9] Xue Y, Bai H, Peng B, Fang B, Baell J, Li L, et al. Stimulus-cleavable chemistry in the field of controlled drug delivery. Chem Soc Rev. 2021; 50: 4872-931.

[10] Dou Y, Li C, Li L, Guo J, Zhang J. Bioresponsive drug delivery systems for the treatment of inflammatory diseases. J Control Release. 2020; 327: 641-66.

[11] Jiang T, Xu G, Chen G, Zheng Y, He B, Gu Z. Progress in transdermal drug delivery systems for cancer therapy, Nano Res. 2020; 13: 1810-24

[12] Hang L, Li H, Zhang T, Men D, Zhang C, Gao P, et al. Au@Prussian Blue Hybrid Nano-material Synergy with Chemotherapeutic Drug for Tumor Diagnosis and Chemo-Dynamic Therapy. ACS Appl Mater Interfaces. 2019; 11: 39493-502.

[13] Li L, Yang Z, Chen X. Recent Advances in Stimuli-Responsive Platforms for Cancer Immunotherapy. Accounts Chem Res. 2020; 53: 2044-2054.

[14] Liu G, Lovell J, Zhang L, Zhang Y. Stimulus-Responsive Nanomedicines for Disease Diagnosis and Treatment. Int J Mol Sci. 2020; 21: 6380

[15] Luo L, Xu F, Peng H, Luo Y, Tian X, Battaglia G, et al. Stimuli-responsive polymeric prodrug-based nanomedicine delivering nifuroxazide and doxorubicin against primary breast cancer and pulmonary metastasis. J Control Release. 2020; 318:

124-35.

[16] Zhou Y, Ye H, Chen Y, Zhu R, Yin L. Photo-Responsive Drug/Gene Delivery Systems, Biomacromolecules 2018; 19: 1840.

[17] Li Z, Hu Y, Miao Z, Xu H, Li C, Zhao Y, et al. Dual-stimuli responsive bismuth nanoraspberries for multimodal imaging and combined cancer therapy. Nano Lett. 2018; 18: 6778-88.

[18] Dong X, Yin W, Zhang X, Zhu S, He X, J. Yu, Xie J, et al. Intelligent MoS_2 nanotheranostic for targeted and enzyme-/pH-/NIR-responsive drug delivery to overcome cancer chemotherapy resistance guided by PET imaging. ACS Appl Mater Interfaces. 2018; 10: 4271-84.

[19] Huang F, Liao W-C, Sohn YS, Nechushtai R, Lu C-H, Willner I. Light-responsive and pH-responsive DNA microcapsules for controlled release of loads. J Am Chem Soc. 2016; 138: 8936-45.

[20] Zhang Y, Zhang Y, Song G, He Y, Zhang X, Liu Y, et al. A DNA–Azobenzene nanopump fFueled by upconversion luminescence for controllable intracellular drug release. Angew Chem Int Ed. 2019; 58: 18207-11.

[21] Zhu K, Liu G, Hu J, Liu S. Near-infrared light-activated photochemical internalization of reduction-responsive polyprodrug vesicles for synergistic photodynamic therapy and chemotherapy. Biomacromolecules. 2017; 18: 2571-82.

[22] Xu Z, Zhang Y, Zhou W, Wang L, Xu G, Ma M, Yang, C. NIR-II-activated biocompatible hollow nanocarbons for cancer photothermal therapy. J Nanobiotechnol. 2021; 19: 1-11.

[23] Jiang Y, Cui D, Fang Y, Zhen X, Pramanik M, Upputuri PK, et al. Amphiphilic semiconducting polymer as multifunctional nanocarrier for fluorescence/photoacoustic imaging guided chemo-photothermal therapy, Biomaterials. 2017; 145: 168-77.

[24] Zhao X, Yang C-X, Chen L-G, Yan X-P. Dual-stimuli responsive and reversibly activatable theranostic nanoprobe for precision tumor-targeting and fluorescence-guided photothermal therapy. Nat Commun. 2017; 8: 1-9.

[25] Song XR, Li SH, Dai J, Song L, Huang G, Lin R, et al. Polyphenol-inspired

facile construction of smart assemblies for ATP-and pH-responsive tumor MR/Optical imaging and photothermal therapy. Small. 2017; 13: 1603997.

[26] Wang X, Xuan Z, Zhu X, Sun H, Li J, Xie Z. Near-infrared photoresponsive drug delivery nanosystems for cancer photo-chemotherapy. J Nanobiotechnol. 2020;18: 1-19.

[27] Zhang X, Wang S, Cheng G, Yu P, Chang J, Chen X. Cascade drug-release strategy for enhanced anticancer therapy. Matter. 2021; 4: 26-53.

[28] Shen S, Ding B, Zhang S, Qi X, Wang K, Tian J,et al. Near-infrared light-responsive nanoparticles with thermosensitive yolk-shell structure for multimodal imaging and chemo-photothermal therapy of tumor. Nanomed Nanotechnol. 2017; 13: 1607-16.

[29] Meng Z, Wei F, Wang R, Xia M, Chen Z, Wang H, et al. NIR-laser-switched in vivo smart nanocapsules for synergic photothermal and chemotherapy of tumors. Adv Mater. 2016; 28: 245-53.

[30] Alkilany AM, Thompson LB, Boulos SP, Sisco PN, Murphy CJ. Gold nanorods: their potential for photothermal therapeutics and drug delivery, tempered by the complexity of their biological interactions. Adv Drug Deliver Rev. 2012; 64: 190-9.

[31] Miao D, Yu Y, Chen Y, Liu Y, Su G. Facile Construction of i-Motif DNA-Conjugated Gold Nanostars as Near-Infrared and pH Dual-Responsive Targeted Drug Delivery Systems for Combined Cancer Therapy. Mol Pharmaceutics. 2020; 17: 1127-38.

[32] Zhou ZH, Liang SY, Zhao TC, Chen XZ, Cao XK, Qi M, Zhong LP. Overcoming chemotherapy resistance using pH-sensitive hollow MnO_2 nanoshells that target the hypoxic tumor microenvironment of metastasized oral squamous cell carcinoma. J Nanobiotechnol. 2021; 19: 1-14.

[33] Tian R, Ke C, Rao L, Lau J, Chen X. Multimodal stratified imaging of nanovaccines in lymph nodes for improving cancer immunotherapy. Adv. Drug Deliver Rev. 2020; 161: 145-160.

[34] Li Volsi A, Scialabba C, Vetri V, Cavallaro G, Licciardi M, Giammona G. Near-infrared light responsive folate targeted gold nanorods for combined

photothermal-chemotherapy of osteosarcoma. ACS Appl Mater Interfaces 2017; 9: 14453-69.

[35] Du Y, Xia L, Jo A, Davis RM, Bissel P, Ehrich MF, et al. Synthesis and evaluation of doxorubicin-loaded gold nanoparticles for tumor-targeted drug delivery. Bioconjugate Chem. 2018; 29: 420-30.

[36] Wang H, Di J, Sun Y, Fu J, Wei Z, Matsui H, et al. Biocompatible PEG-chitosan@carbon dots hybrid nanogels for two-photon fluorescence imaging, near-infrared light/pH dual-responsive drug carrier, and synergistic therapy. Adv Funct Mater. 2015; 25: 5537-47.

[37] Cheng L, Wang C, Feng L, Yang K, Functional nanomaterials for phototherapies of cancer. Chem Rev. 2014; 114: 10869-939.

[38] Song S, Chong Y, Fu H, Ning X, Shen H, Zhang Z. HP-β-CD functionalized Fe_3O_4/CNPs-based theranostic nanoplatform for ph/nir responsive drug release and mr/nirfl imaging-guided synergetic chemo/photothermal therapy of tumor. ACS Appl Mater Interfaces. 2018; 10: 33867-78.

[39] Ku G, Zhou M, Song S, Huang Q, Hazle J, Li C. Copper sulfide nanoparticles as a new class of photoacoustic contrast agent for deep tissue imaging at 1064 nm. ACS Nano. 2012; 6: 7489-96.

[40] Han L, Zhang Y, Chen X-W, Shu Y, Wang J-H. Protein-modified hollow copper sulfide nanoparticles carrying indocyanine green for photothermal and photodynamic therapy. J Mater Chem B. 2016; 4: 105-12.

[41] Guo L, Panderi I, Yan D, Szulak K, Lu W. A comparative study of hollow copper sulfide nanoparticles and hollow gold nanospheres on degradability and toxicity. ACS Nano. 2013; 7: 8780.

[42] Zhang C, Men D, Zhang T, Yu Y, Xiang J, Jiang G, et al. Nanoplatforms with remarkably enhanced absorption in the second biological window for effective tumor thermoradiotherapy. ACS Appl Mater Interfaces. 2019; 12: 2152-61.

[43] Fang Y, Luan D, Chen Y, Gao S, Lou XW. Synthesis of copper-substituted CoS_2@CuxS double-shelled nanoboxes by sequential ion exchange for efficient sodium storage. Angew Chem. 2020;132(7):2666-70.

[44] Garg AD, Krysko DV, Verfaillie T, Kaczmarek A, Ferreira GB, Marysael T, et al. A novel pathway combining calreticulin exposure and ATP secretion in immunogenic cancer cell death. EMBO J. 2012; 31: 1062-79.

[45] Aymeric L, Apetoh L, Ghiringhelli F, Tesniere A, Martins I, Kroemer G, et al. Tumor cell death and ATP release prime dendritic cells and efficient anticancer immunity. Cancer Res. 2010; 70: 855-8.

[46] Obeid M, Tesniere A, Ghiringhelli F, Fimia GM, Apetoh L, Perfettini JL, et al. Calreticulin exposure dictates the immunogenicity of cancer cell death. Nat Med. 2007; 13: 54-61.

[47] Sang W, Zhang Z, Dai Y, Chen X. Recent advances in nanomaterial-based synergistic combination cancer immunotherapy. Chem Soc Rev. 2019; 48: 3771-810.

[48] Kepp O, Senovilla L, Vitale I, Vacchelli E, Adjemian S, Agostinis P, et al. Consensus guidelines for the detection of immunogenic cell death. Oncoimmunology. 2014; 3: e955691.

[49] Zhang C, Men D, Zhang T, Yu Y, Xiang J, Jiang G, et al. Nanoplatforms with remarkably enhanced absorption in the second biological window for effective tumor thermoradiotherapy. ACS Appl Mater Interfaces. 2019; 12: 2152-61.

Supplementary Files

This is a list of supplementary files associated with this preprint. Click to download.

- Graphicalabstractimage.png
- SupplementaryMaterial.docx